Laser effects in photoionization: Numerical solution for a one-dimensional δ potential

K. J. LaGattuta
Los Alamos National Laboratory, Mail Stop B-257, Los Alamos, New Mexico 87545
(Received 14 November 1988; revised manuscript received 13 March 1989)

The time-dependent Schrödinger equation was solved numerically, in one spatial dimension, for an electron bound initially ($t<0$) by a δ potential, and acted upon by a single-frequency classical electromagnetic field, turned on abruptly at $t=0$. The dipole approximation was invoked for the laser field, and magnetic interactions were ignored. Characteristic photoionization times were determined for a wide range of scaled laser intensities and scaled laser frequencies. The conditions under which well-defined quiver motion of the ionizing electron appears were clarified, and a spectrum of radiation emitted during the ionization process was determined. Above-threshold-ionization spectra of ionized electrons were also computed.

INTRODUCTION

The time-dependent Schrödinger equation was solved numerically, in one spatial dimension, for an electron bound initially ($t>0$) by a δ potential, and acted upon by a single-frequency classical electromagnetic field, turned on abruptly at $t=0$. The dipole approximation was invoked for the laser field, and magnetic interactions were ignored.

Values were obtained for the time-dependent photoionization probability $P_{\rm ion}(t)$ and characteristic photoionization time $\tau_{\rm PI}$ over a wide range of laser intensities ($I_0>0$) and frequencies ($\omega_0>0$), and for a wide range of electron binding energies ($E_B>0$). An exact scaling relationship was applied which reduced these three parameters (I_0, ω_0, E_B) to just two (I_0' and ω_0'), where $I_0'\equiv I_0/(8E_B^3)$ and $\omega_0'\equiv\omega_0/(2E_B)$ Time and space variables were thereby also scaled; e.g., $\tau_{\rm PI}'\equiv(2E_B)\tau_{\rm PI}$.

The conditions under which well-defined quiver motion of the ionizing electron occurs were clarified, and the spectral density of energy radiated during ionization was computed. An above-threshold-ionization (ATI) spectrum of kinetic energies was also determined for the emitted electrons, and ponderomotive shifts were observed.

Comparison of these explicit and computer intensive calculations for $\tau_{\rm PI}'$, with predictions made by three approximate and computationally very rapid methods, suggested that if (1) $I_0'<\omega_0'^2$, and $I_0'<1$, then the Reiss approximation[1] was adequate [that is, the analog of the Reiss approximation, specific to the one-dimensional δ potential; see Eq. (45)]; (2) $I_0'>1$, then a semiclassical wave-packet description was successful; (3) $\omega_0'^2<I_0'<1$, then a field-ionization formula could be applied with some success, particularly when $\omega_0'^2\ll I_0'$; see Fig. 1.

The computational method, to be described, is straightforward and generalizable to more complicated systems. Elements of the method have been employed previously by several groups[2–5] for related purposes; see especially the work reported in Ref. 2. Somewhat different approaches to the problem of photoionization by intense lasers have also been described recently.[6–8]

The modeling, by use of the plasma-kinetics codes such as ZAP (Ref. 9) used at Los Alamos National Laboratory (LANL), of the interaction of atomic gases with short-pulse, high-intensity lasers, requires detailed knowledge of photoionization rates for a wide range of laser intensities and frequencies, and electron binding energies. In a typical pulse of the LANL Bright Source KrF laser,[10,11] intensities in excess of 10^{17} W/cm^2 are reached, for times of the order of 1 psec, at a wavelength of ~250 nm. Under such conditions, target gas atoms are stripped to high stages of ionization, presumably via sequential[12] (outer shells first) direct multiphoton absorption.

Impact ionization of an inner-shell electron via collision with a rapidly quivering outer-shell electron is possible, in principle, at very high laser intensities.[13] Also, direct inner-shell multiphoton photoionization might occur. For the high-intensity KrF laser, however, these processes have not been observed.[11]

Presently, a generally accurate predictor of high-intensity laser-induced photoionization rates is unavailable. The sometimes applied Reiss[1] formula (or its analog) has been shown to be reliable only over a limited region of parameter (I_0,ω_0,E_B) space.[6,14]

The goal of the present study was to obtain rough estimates of the characteristic time for direct photoionization of a bound electron $\tau_{\rm PI}$ as a function of I_0, ω_0, and E_B, for as large a range of I_0, ω_0, and E_B as possible. In a plasma-kinetics code, $\tau_{\rm PI}$ affects the population of a

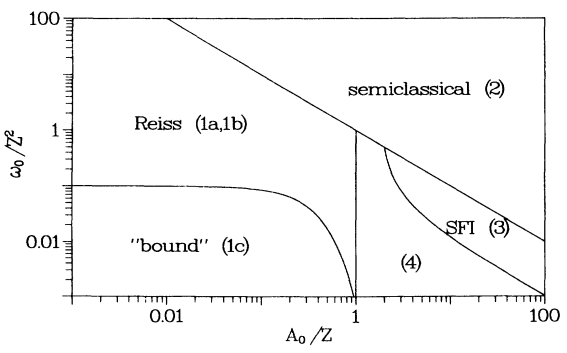

FIG. 1. ω_0' vs A_0'. Regions of parameter space: numbers 1–3 correspond to cases in the Results section, also see the Discussion section.

 ©1989 The American Physical Society

given atomic or ionic bound-electronic level according to

$$dN_B(t)/dt = -(1/\tau_{\rm PI})N_B + \cdots , \quad (1)$$

where $N_B(t)$ is the population, at time t, of the bound level labeled by B, and terms involving depletion (or repopulation) mechanisms other than direct photoionization are denoted by the ellipsis. The cumulative photoionization probability $P_{\rm ion}(t)$ is related to the instantaneous level population $N_B(t)$ via

$$N_B(t) = N_B(0)[1 - P_{\rm ion}(t)] \equiv N_B(0)P_B(t) , \quad (2)$$

where $P_B(t) = 1 - P_{\rm ion}(t)$ is the probability of remaining in the bound level labeled by B.

It may be that the roll-off of $P_B(t)$ is not very well described by just a single exponential factor, or by any finite combination of exponential factors. For example, when $I_0 \gg 1$ it can happen that $P_B(t) \sim 1/t$, so that Eq. (1) will hold only in a rough qualitative sense. This point will be discussed further in the Results section (case 2).

For the application described, we have assumed that the dominant bound-state characteristic affecting $\tau_{\rm PI}$ in Coulomb systems is the binding energy E_B. Moreover, we have assumed that results obtained for the one-dimensional δ potential will provide an order of magnitude estimate of the corresponding rates for electrons bound by real three-dimensional (3D) ions, when acted upon lasers with linear polarization. In certain cases, this may be a poor assumption; e.g., near photoionization thresholds. See further remarks in the Discussion section.

FORMALISM

The Schrödinger equation, for the system of an electron bound initially ($t < 0$) by a δ potential, and acted upon for $t \geq 0$ by a single-frequency classical electromagnetic field is, in atomic units (a.u.) and in the $\mathbf{k}\cdot\mathbf{A}$ gauge,

$$\left[-\frac{1}{2}\frac{d^2}{dx^2} - Z\delta(x) - iA(t)\frac{d}{dx} + \tfrac{1}{2}A^2(t) - \frac{id}{dt} \right] \times \Psi(x,t) = 0 , \quad (3)$$

where the coupling constant, $Z > 0$, measures the strength of the static (binding) potential. The vector potential was taken to be

$$A(t) = A_0[\sin(\omega_0 t + \phi) - \sin\phi]\Theta(t), \quad -\pi \leq \phi \leq \pi \quad (4)$$

where ϕ is an arbitrarily chosen phase and $\Theta(t)$ is the unit step function [$\Theta(t) = 1$ for $t \geq 0$, $\Theta(t) = 0$ for $t < 0$]. In Eq. (3), the dipole approximation has been made for the electromagnetic (EM) field, and magnetic interactions have been ignored. The time-averaged laser irradiance I_0 is related to the amplitude of the vector potential A_0 by $I_0 = A_0^2\omega_0^2$. (1 a.u. of time-averaged irradiance equals 3.54×10^{16} W/cm^2.)

The vector potential $A(t)$ is related to the laser electric field strength $E(t)$ by

$$E(t) = -\frac{dA(t)}{dt} = -A_0\omega_0\cos(\omega_0 t + \phi)\Theta(t) . \quad (5)$$

Recall that the vector potential can only be defined up to an arbitrary constant. We chose this constant to be equal to zero; i.e., $A(0) = 0$.

With this choice of initial value for $A(t)$, the Schrödinger equation for $t < 0$ may be written as

$$\left[-\frac{1}{2}\frac{d^2}{dx^2} - Z\delta(x) - \varepsilon \right]\phi(x) = 0 , \quad (6)$$

with bound solution

$$\phi_B(x) = C_B\exp(-Z|x|) , \quad (7)$$

eigenvalue $\varepsilon_B = -Z^2/2$ ($E_B \equiv -\varepsilon_B$), and normalization constant C_B [Eq. (12)]. The continuum solutions of Eq. (6) were chosen such that

$$\phi_k(x) = C_k\{\exp(ikx) - (Z/k)[1/(1+Z^2k^2)^{1/2}]\sin(k|x|) + [1/(1+Z^2/k^2)^{1/2} - 1]\cos(kx)\} , \quad (8)$$

with eigenvalues $\varepsilon_k = k^2/2$ and normalized in a box of length $2L$, centered at the origin. Under these conditions, the continuum normalization constant C_k is independent of k; viz.,

$$C_k = 1/\sqrt{2L} , \quad (9)$$

and the continuum wave vectors k have the values

$$k = n\pi/L , \quad (10)$$

where n is an integer (either positive or negative, but not zero). As given in Eq. (8), the continua are normalized in the momentum scale; i.e.,

$$\int dx\, \phi^*_{k'}(x)\phi_k(x) = 2\pi\delta_{kk'} , \quad (11)$$

where the range of the integral extends from $-L$ to L, and where $\delta_{kk'}$ is the Kronecker delta. For $Z \to 0$, the ϕ_k go over into box-normalized plane waves. In a box of length $2L$, the bound state [Eq. (7)] normalization constant is given by

$$C_B = Z/(1 - e^{-2ZL})^{1/2} , \quad (12)$$

so that $C_B = Z$, if $ZL \gg 1$.

For $t \geq 0$, the wave function solution of Eq. (3) was expanded in eigenstates of Eq. (6) according to

$$\Psi(x,t) = a_B(t)\phi_B(x)\exp(-i\varepsilon_B t) + \sum_k a_k(t)\phi_k(x)\exp(-i\varepsilon_k t) . \quad (13)$$

Then, upon substitution of Eq. (13) into Eq. (3), the Schrödinger equation transformed into a set of coupled first-order ordinary linear differential equations[3] for the time-dependent coefficients $a_B(t)$ and $a_k(t)$, which we write concisely as

$$\frac{da_j(t)}{dt} = \sum_{j'} U_{jj'}(t)a_{j'}(t) , \quad (14)$$

where j enumerates both the bound and continuum states, and subject to the initial conditions

$$|a_B(0)|=1 \ , \tag{15}$$

$$a_k(0)=0 \quad \text{for all } k \ .$$

The $U_{jj'}(t)$ are given by

$$U_{jj'}(t)=-A(t)\exp[i(\varepsilon_j-\varepsilon_{j'})t] \times \int dx\, \phi_j^*(x)(d/dx)\phi_{j'}(x) - i\tfrac{1}{2}A^2(t)\delta_{jj'} \tag{16}$$

and satisfy the symmetry (anti-hermiticity) relationship

$$U_{jj'}(t)+U_{j'j}^*(t)=0 \tag{17}$$

while the $a_j(t)$ obey the time-independent normalization condition

$$\sum_j |a_j(t)|^2=1 \ . \tag{18}$$

Equation (14) was solved numerically for the $a_j(t)$, subject to the initial conditions of Eq. (15). Then the probability of remaining in the bound state, for any $t\geq 0$, was found by projecting the full wave function $\Psi(x,t)$ onto the bound solution of Eq. (6), obtained for zero electric field

$$P_B(t)=\left|\int dx\, \phi_B^*(x)\exp[ixA(t)]\Psi(x,t)\right|^2 \tag{19}$$

while the probability of appearing in a continuum state was given by

$$P_k(t)=\left|\int dx\, \phi_k^*(x)\exp[ixA(t)]\Psi(x,t)\right|^2 . \tag{20}$$

Note that a zero of the electric field is not generally synonomous with a zero of the vector potential. Therefore, the solutions of Eq. (6), obtained for $A(t)=0$ [Eqs. (7) and (8)], must all be multipled by the phase factor $\exp[-ixA(t)]$, wherever either $P_B(t)$ or $P_k(t)$ is to be determined. That is, the true basis states in $\mathbf{k}\cdot\mathbf{A}$ gauge, for any time $t\geq 0$, are not given by the solutions of Eq. (6), but are the solutions of Eq. (3), with $A(t)$ treated as a constant. See Ref. 15 and the following section (Gauge Dependence) for further information.

The spectrum of emitted electron energies, $P_k(t)$ in Eq. (20), oscillates in time with frequency ω_0, with the probabilities corresponding to positive and negative k values being out of phase by π. Laboratory experiments[16] in which such spectra have been measured detect electrons in a region of space where the laser has zero intensity.[6] For comparison with such experiments, $P_k(t)$ should be evaluated at the times $t_m=2m\pi/\omega_0$, where m is any positive integer (but $t_m\gg\tau_{\rm PI}$); i.e., the times at which $A(t)=0$.

We note that the nominal basis described in this section [solutions of Eq. (6)] is most appropriate when the laser intensity is low. Generally, as the laser intensity increases, one expects that the amount of mixing among the continuua [Eq. (8)] will increase, since the laser distorts those continua. See the Volkov State Basis section for further discussion of this point. Other difficulties which occur at high intensities are (a) the range of k values [maximum n value, in Eq. (10)] must be increased, since the electron absorbs energy from the laser, and (b) the minimum k value (π/L) must be decreased, in order to prevent the most rapidly moving components of the electron wave function from reaching the end of the "box." In the worst case, when both $I_0\gg\omega_0^2$ and $I_0\ll 1$, then the effects cited in both a and b lead to severe computational loading, since now photoionization proceeds very slowly, yet large time-varying electron-quiver energies, $A^2(t)/2$, are generated, mandating very small time steps.

GAUGE DEPENDENCE

A gauge (unitary) transformation[15] can be applied to Eq. (3), changing the form of the interaction between electron and EM field from the $\mathbf{k}\cdot\mathbf{A}$ to the $\mathbf{x}\cdot\mathbf{E}$ gauge. From Eqs. (3) and (4), the Schrödinger equation becomes, in $\mathbf{x}\cdot\mathbf{E}$ gauge,

$$\left[-\frac{1}{2}\frac{d^2}{dx^2}-Z\delta(x)+xE(t)-i\frac{d}{dt}\right]\tilde{\Psi}(x,t)=0 \ , \tag{21}$$

where $E(t)$ appears in Eq. (5). The wave function in the $\mathbf{x}\cdot E$ gauge, $\tilde{\Psi}$, is related to the wave function in the $\mathbf{k}\cdot\mathbf{A}$ gauge, Ψ, by

$$\tilde{\Psi}(x,t)\equiv\exp[ixA(t)]\Psi(x,t) \ . \tag{22}$$

Obviously, one has for the probability density dP/dx that

$$\frac{dP(x,t)}{dx}\equiv|\tilde{\Psi}(x,t)|^2=|\Psi(x,t)|^2 \ , \tag{23}$$

independent of gauge, for all x and t.

In analogy to Eq. (13), one may expand the solution of Eq. (21) as

$$\tilde{\Psi}(x,t)=\tilde{a}_B(t)\phi_B(x)\exp(-i\varepsilon_B t) + \sum_k \tilde{a}_k(t)\phi_k(x)\exp(-i\varepsilon_k t) \ . \tag{24}$$

The analog of Eq. (14) is then

$$\frac{d\tilde{a}_j(t)}{dt}=\sum_{j'}\tilde{U}_{jj'}(t)\tilde{a}_{j'}(t) \ , \tag{25}$$

where

$$\tilde{U}_{jj'}(t)=iA_0\omega_0\cos(\omega_0 t+\phi)\Theta(t)\exp[i(\varepsilon_j-\varepsilon_{j'})t] \times\int dx\, \phi_j^*(x)x\phi_{j'}(x) \tag{26}$$

while the $\tilde{U}_{jj'}$ satisfy the relationship

$$\tilde{U}_{jj'}(t)+\tilde{U}_{j'j}^*(t)=0 \ . \tag{27}$$

The probability of remaining in the bound state [Eq. (19)] can now be written as

$$P_B(t)=\left|\int dx\, \phi_B^*(x)\tilde{\Psi}(x,t)\right|^2=|\tilde{a}_B(t)|^2 \tag{28}$$

while the probability of occupying a continuum level [Eq. (20)] becomes

$$P_k(t)=\left|\int dx\ \phi_k^*(x)\tilde{\Psi}(x,t)\right|^2 = |\tilde{a}_k(t)|^2 \ . \tag{29}$$

Thus, once having obtained $\tilde{\Psi}$, the computation of $P_B(t)$ is more expeditious in the $\mathbf{x}\cdot\mathbf{E}$ gauge than in the $\mathbf{k}\cdot\mathbf{A}$ gauge; i.e., only a knowledge of $\tilde{a}_B(t)$ is required. However, as will be discussed, a computation of $\tilde{\Psi}$ is usually more time consuming than one of Ψ, for an identical choice of laser parameters. Note that, generally, $|\tilde{a}_B(t)|^2 \neq |a_B(t)|^2$, and $|\tilde{a}_k(t)|^2 \neq |a_k(t)|^2$.

SCALING

The solutions of Eq. (3) depend formally on the parameters A_0, ω_0, and Z. However, the Z dependence can be scaled away. That is, after dividing all terms on the right-hand-side of Eq. (3) by Z^2, one is left with a Z independent equation, in the $\mathbf{k}\cdot\mathbf{A}$ gauge, of the form

$$\left[-\frac{1}{2}\frac{d^2}{dx'^2}-\delta(x')-iA'(t')\frac{d}{dx'} +\tfrac{1}{2}A'^2(t')-i\frac{d}{dt'}\right]\Psi(x',t') \ , \tag{30}$$

where the scaled quantities, denoted by primes, are defined by

$$\begin{aligned} A_0' &= A_0/Z \ , \\ \omega_0' &= \omega_0/Z^2 \ , \\ x' &= Zx \ , \\ t' &= Z^2 t \ . \end{aligned} \tag{31}$$

The scaled eigenvalues of the unperturbed time-independent Schrödinger equation [Eq. (6)] are

$$\begin{aligned} \varepsilon_B' &= -\tfrac{1}{2} \ , \\ \varepsilon_k' &= k'^2/2 = k^2/(2Z^2) \ , \end{aligned} \tag{32}$$

where k values are still given by Eq. (10).

In practice, Eq. (30) or its analog in the $\mathbf{x}\cdot\mathbf{E}$ gauge was solved for a range of A_0' and ω_0' values. Solutions of Eq. (30) correspond directly to solutions of Eq. (3) when $Z=1$. For other values of Z, recourse was had to the scaling relations of Eq. (31). Through these scaling relations, solutions for any A_0, ω_0, and Z combination could be derived from results obtained over a range of A_0' and ω_0'.

To illustrate, from data described in the Results section, obtained for $A_0'=8.0$ and $\omega_0'=0.04$ [case (3)], and for which the computed characteristic photoionization time was $\tau_{\rm PI}'\approx 9.7$, we compiled the entires of Table I. (1 a.u., of time equals 2.42×10^{-17} sec.)

TABLE I. Values of $\tau_{\rm PI}$ obtained for case (3), when $Z=1$, 2, and 3. $A_0'=8.0$, $\omega_0'=0.04$, and $\phi=0.0$.

Z	ε_B (eV)	ω_0 (eV)	I_0 (W/cm^2)	$\tau_{\rm PI}$ (fsec)
1	−13.6	1.1	3.6×10^{15}	0.23
2	−54.4	4.4	2.3×10^{17}	0.059
3	−122.5	9.8	2.6×10^{18}	0.026

VOLKOV STATE BASIS

When the laser intensity is high, then the basis described in the Formalism section [eigenstates of Eq. (6)] may be inappropriate. As the laser intensity increases, distortion of the continuum solutions of Eq. (6) will increase. Therefore, the range of k values over which important continuum-continuum coupling occurs will also increase [range of j' sum in Eq. (14)]. The required computer time thereby increases very rapidly.

To facilitate the description of such cases, we invoked a basis of modified Volkov (nonrelativistic) states.[17] These are the solutions of

$$\left[-\frac{1}{2}\frac{d^2}{dx^2}-iA(t)\frac{d}{dx}-i\frac{d}{dt}\right]\Lambda(x,t)=0 \ , \tag{33}$$

labeled by k according to

$$\Lambda_k(x,t)=(1/\sqrt{2L}\,)\exp\{ik[x-x_0(t)]-k^2t/2\} \tag{34}$$

and normalized in a box of length $2L$. Then, k takes on the discrete values given by Eq. (10). The "trajectory function" $x_0(t)$ appears in Eq. (47). As defined, the basis of modified Volkov states is orthornormal and complete on the interval $-L\le x\le L$.

The solution of Eq. (3) ($\mathbf{k}\cdot\mathbf{A}$ gauge) is expanded in the Λ_k as

$$\Psi(x,t)=\sum_k \lambda_k(t)\Lambda_k(x,t) \tag{35}$$

and, in the usual way, an equation for the λ_k is obtained,

$$\frac{d\lambda_k(t)}{dt}=\sum_{k'} V_{kk'}(t)\lambda_{k'}(t) \ . \tag{36}$$

The $V_{kk'}$ are given by

$$V_{kk'}(t)=i(Z/2L)\exp[i(k-k')x_0(t) +i(k^2-k'^2)t/2]\Theta(t) -i\tfrac{1}{2}A^2(t)\delta_{kk'} \ . \tag{37}$$

In the modified Volkov basis, the probability of remaining in the bound state is

$$P_B(t)=\left|\int dx\,\phi_B^*(x)\exp[ixA(t)]\Psi(x,t)\right|^2$$
$$=(Z/2L)\left|\sum_{k'}\lambda_{k'}(t)\exp(-ik'^2t/2)\int dx\,\exp(-Z|x|)\exp\{ik'[x-x_0(t)]+ixA(t)\}\right|^2 \quad (38)$$
$$=(2Z^3/L)\left|\sum_{k'}\lambda_{k'}(t)\exp[-ik'x_0(t)-ik'^2t/2](1/\{Z^2+[k'+A(t)]^2\})\right|^2 ,$$

where the bound-state wave function $\phi_B(x)$ is given by Eq. (7), and terms of order e^{-ZL} are ignored.

Since one has that , initially,

$$\phi_B(x)=(1/\sqrt{2L})\sum_{k'}\lambda_{k'}(0)\exp(ik'x) , \quad (39)$$

then the initial values of the $\lambda_k(t)$ are given by

$$\lambda_k(0)=(2Z^3/L)^{1/2}[1/(Z^2+k^2)] \quad (40)$$

up to terms of order e^{-ZL}.

RESULTS

An exhaustive set of calculations of $P_B(t')$, as defined in Eq. (28) and based on Eq. (30), for a wide range of $A_0'>0$ and $\omega_0'>0$ values has shown that photoionization behavior may usefully be divided, into three regions of (I_0',ω_0') parameter space. These regions are (1) $I_0'<1$ and $I_0'<\omega_0'^2$, where the Reiss approximation[1] [Eq. (45)] was adequate; (2) $I_0'>1$, where a semiclassical wave-packet description sufficed; (3) $I_0'<1$ and $I_0'>\omega_0'^2$, where a field ionization formula could be applied; see Fig. 1. We will now consider each of these regions of parameter space in turn. Unless otherwise specified, calculations reported in this section, have all been performed with the phase $\phi=0$ [Eq. (4)]. Also, recall that $I_0'=A_0'^2\omega_0'^2$.

Case (1): Reiss approximation ($I_0'<1$ and $I_0'<\omega_0'^2$)

We further divide this region into three parts, as follows

Case 1(a): If $\omega_0'>0.5$

Here, one photon may suffice to produce ionization, provided that I_0' is small enough. "Small enough" means generally that the ponderomotive shift,[16] when added to the binding energy should not exceed the photon energy. In scaled units, this implies that

$$\omega_0'>\tfrac{1}{2}+A_0'^2/4 . \quad (41)$$

We are now in the region of validity of the first Born approximation (FBA); i.e., when the coupling between the electron and the laser field acts only once, although the electron interacts with the binding potential to all orders. A transition is induced between this exact bound state [Eq. (7)] and an exact continuum state [Eq. (8)] via one-photon absorption. The FBA is the limit, for $\omega_0'>0.5$ and $A_0'\to 0$, of the one-dimensional Reiss approximation; see case 1 (b).

For ionization of the initially bound state, the characteristic transition time is given in the FBA, and in scaled units, by

$$1/\tau_{\rm PI}'=2|k'|A_0'^2/(1+k'^2)^2 , \quad (42)$$

where the energy-conserving k' value satisfies

$$k'^2=2(\omega_0'-\tfrac{1}{2}-A_0'^2/4) . \quad (43)$$

As an example, we display in Fig. 2 the results of a calculation of $P_B(t')$ versus t', based on Eq. (28), and for $A_0'=0.25$ and $\omega_0'=0.6$. In the FBA [Eq. (42)], the predicted value of the ionization time is $\tau_{\rm PI}'=26$, while from Fig. 2, $P_B(t')=1/e$, when $t'=32$. The $\sim 25\%$ discrepancy between the FBA value of $\tau_{\rm ion}'$ and the "measured" value decreases as A_0' decreases.

The corresponding spectrum of emitted electrons $[P_{k'}(t')$ versus $k'^2/2]$, for $t'=28\pi/\omega_0'>\tau_{\rm PI}'$, appears in Fig. 3. The most likely energy, $k'^2/2\sim 0.08$, is consistent with Eq. (43) which predicts $k'^2/2=0.084$. Smaller peaks in the emitted-electron spectrum occur also at $k'^2/2\sim 0.68$, 1.28, and 1.88. These are the so-called ATI peaks,[16] which appear here even at these low field intensities. (But, note that the ordinate scale is logarithmic.)

In Fig. 4, we plot the probability density $|\Psi(x',t')|^2$ versus x' [see Eq. (23)] for $t'=0$, 50, 100, and 150. Note that, for this choice of A_0' and ω_0', the electron is emitted with almost equal probability in both the positive and negative x' directions. (There is a slight excess of probability in the negative x' direction, as indicated by the average x' value at this time.) Now, the center of the wave packet, on each side of the origin, is seen to have moved $\sim 45-50$ a.u. of distance from the origin, in 150 a.u. of time. This implies a kinetic energy of $\sim 0.045-0.056$ a.u. which is less than the most likely energy of ~ 0.08, appearing in Fig. 3. However, in making

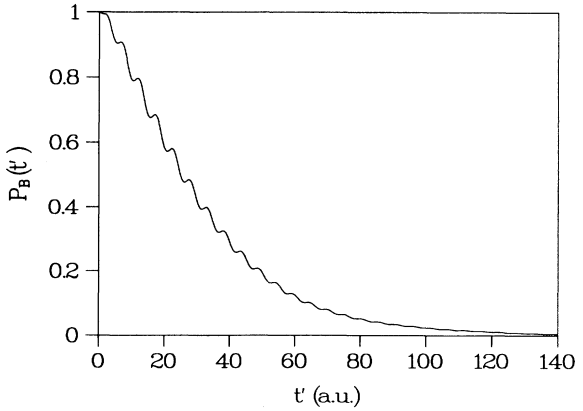

FIG. 2. $P_B(t')$ vs t', for $A_0'=0.25$, $\omega_0'=0.6$, and $\phi=0$.

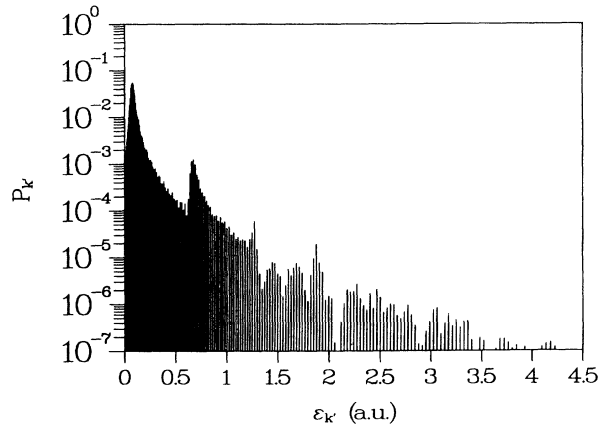

FIG. 3. $P_{k'}(k')$ vs $k'^2/2$, at $t'=28\pi/\omega_0'$; conditions as in Fig. 2.

this comparison one must take into account the "delay time" which transpires before emission, which is of the order of $\tau'_{\rm ion}\sim 32$ a.u. Consequently, the electron has actually been "moving" in the continuum for a time of the order of 120 a.u. The estimated kinetic energy is now indeed ~ 0.08 a.u.

In Fig. 5, we plot the expectation value of the electron coordinate x' at t'; i.e.,

$$\langle x'\rangle(t')=\int dx'\Psi^*(x',t')x'\Psi(x',t') = \int dx'\tilde{\Psi}^*(x',t')x'\tilde{\Psi}(x',t') \ . \tag{44}$$

Notice that for $t'>\tau'_{\rm PI}$, $\langle x'\rangle(t')$ undergoes oscillations with period $\sim 2\pi/\omega_0'$ and amplitude $\sim A_0'/\omega_0'$, while drifting toward negative x' values with a nearly constant velocity. Concerning this drift, see the remarks following Eq. (56).

Case (1b): $0.1<\omega_0'<0.5$

In this case, multiphoton processes will occur in leading order. However, the field intensity is still low, so that ionization is "slow;" i.e., $\tau'_{\rm PI}\gg 2\pi/\omega_0'$. A generalization of the nth Born approximation,[2] developed by Reiss,[1] was observed to hold under these circumstances. In the Reiss approach, the electron first absorbs one photon, making a

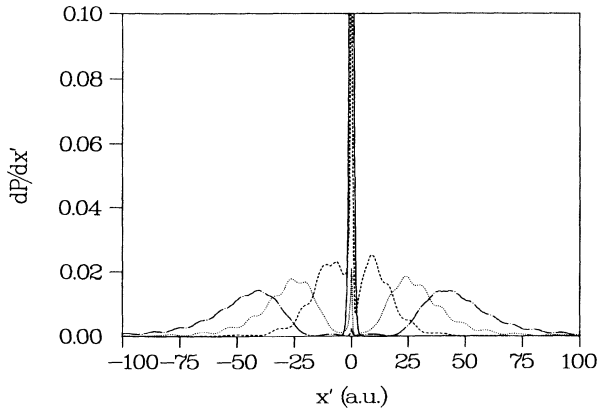

FIG. 4. $|\Psi(x',t')|^2$ vs x' for $t'=0$(——), 50(— — —), 100(· · · ·), and 150(—·—·—·); conditions as in Fig. 2.

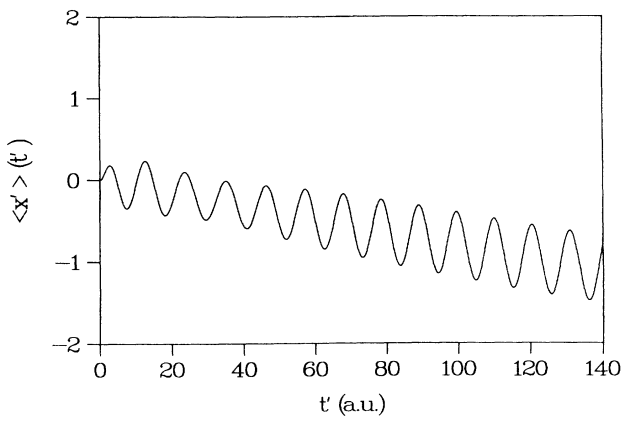

FIG. 5. $\langle x'\rangle(t')$ vs t'; conditions as in Fig. 2.

transition from the bound state [Eq. (7)] into the plane-wave continuum. Subsequently, additional photons are absorbed but the electron is forced to remain throughout in the same plane-wave continuum state. This is tantamount to the electron's making a direct transition from the bound state into a (nonrelativistic) Volkov state.[17] The predicted decay time for this process is given by

$$1/\tau'_{\rm PI}=8\omega_0'^2\sum_{l(>l_0)}(1/|k_l'|)\{1/[1+(k_l')^2]^2\}J_l^2(|k_l'|A_0'/\omega_0') \tag{45}$$

for the δ potential, where J_l is the ordinary Bessel function of order l (l is a real and positive integer), and

$$(k_l')^2=2[l\omega_0'-\tfrac{1}{2}-(A_0')^2/4] \ . \tag{46}$$

The sum in Eq. (45) begins with the smallest integer l_0 such that the right-hand side of Eq. (46) is positive. In Eq. (45), it is tacitly assumed that $\tau'_{\rm PI}\gg 2\pi/\omega_0'$; i.e., that A_0' is not "too large." If $A_0'\ll 1$, and $\omega_0'>0.5$, then the Reiss approximation reduces to the FBA.

As an example, in Fig. 6 we plot $P_B(t')$ versus t' for the case $A_0'=0.5$ and $\omega_0'=0.4$. $P_B(t')$ falls to $1/e$ for $t'\sim 130$, while Eq. (45) predicts $\tau'_{\rm PI}=140$. The corresponding spectrum of emitted electron energies appears in Fig. 7. The leading order in the spectrum (lowest continuum energy) occurs for $l=l_0=2$, and has a value

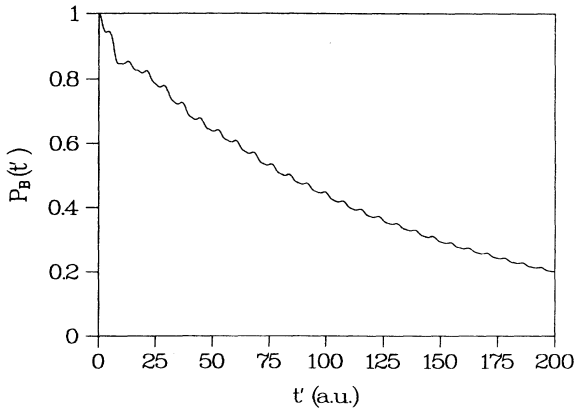

FIG. 6. $P_B(t')$ vs t', for $A_0'=0.5$, $\omega_0'=0.4$, and $\phi=0$.

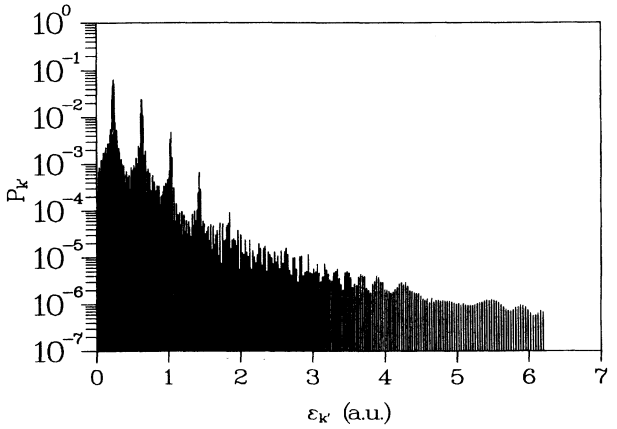

FIG. 7. $P_{k'}(k')$ vs $k'^2/2$, at $t'=26\pi/\omega_0'$; conditions as in Fig. 6.

$k_n'^2/2=0.23$, consistent with Eq. (46), which predicts $k'^2/2=0.24$. ATI peaks are visible at $k'^2/2=0.63$, 1.03, and 1.43.

In Fig. 8, we plot the probability density $|\Psi(x',t')|^2$ versus x' for $t'=200>\tau_{\rm PI}'$. As in case (1a), the probability of electron emission is almost symmetrical about $x'=0$, with a slight excess of probability in the negative x' direction. In Fig. 9, we plot the expectation value of x' at t'; i.e., from Eq. (44). Again as in case (1a), one sees that, for $t'>\tau_{\rm PI}'$, $\langle x'\rangle(t')$ undergoes oscillations with period $\sim 2\pi/\omega_0'$ and amplitude $\sim A_0'/\omega_0'$, while drifting toward negative x' values with a nearly constant velocity.

Case (1c): $\omega_0'<0.1$

In this case, values of $\tau_{\rm PI}'$, as determined by the Reiss formula [Eq. (45)], become very large, typically exceeding 1 sec, and are thereby uninteresting from a laser-plasma modeling point of view. We propose to regard such electrons as bound ($\tau_{\rm PI}'\to\infty$).

Case (2): Semiclassical approximation ($I_0'>1$)

Choosing $A_0'=30$ and $\omega_0'=5$, one has the result displayed in Fig. 10, for $P_B(t')$ versus t'. Ionization is "slow," in that $\tau_{\rm PI}'>2\pi/\omega_0'$. The envelope of the $P_B(t')$ curve falls to $1/e$ in a time $t'\sim 35$. However, the falloff is not exponential.

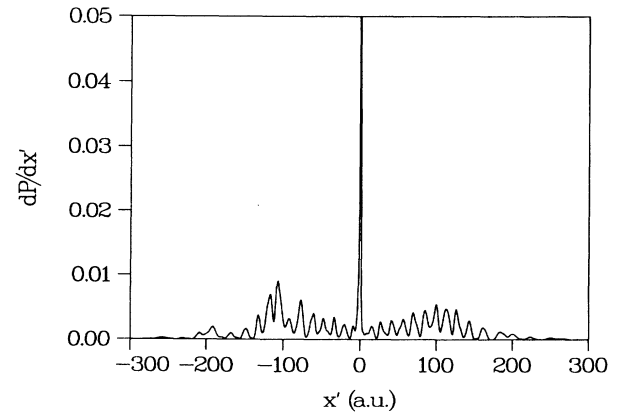

FIG. 8. $|\Psi(x',t')|^2$ vs x', for $t'=200$; conditions as in Fig. 6.

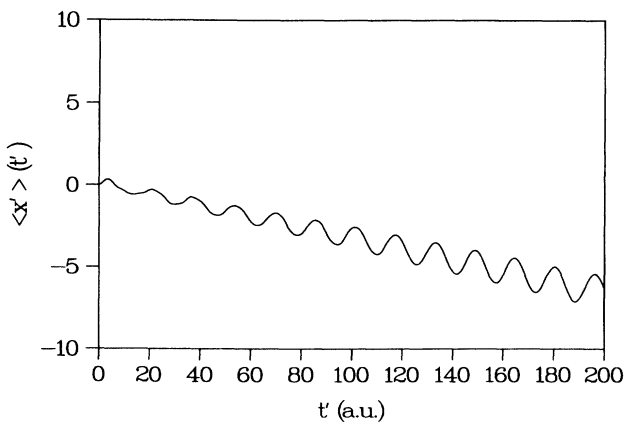

FIG. 9. $\langle x'\rangle(t')$ vs t'; conditions as in Fig. 6.

In this strongly coupled case, pronounced dipole charge-density oscillations occur. In Fig. 11, we plot values of the probability density $|\Psi(x',t')|^2$ versus x', for $t'=0$, π/ω_0', and $2\pi/\omega_0'$. As t' increases further the wave packet spreads. Finally, in Fig. 12, we plot values of the expectation value of x' versus t'. It is clear from Figs. 11 and 12 that, to a good approximation, for all $t'>0$, the electron oscillates between $x'=0$ and $x'=A_0'/\omega_0'$, with period $2\pi/\omega_0'$, according to the law

$$x'(t')=(A_0'/\omega_0')[1-\cos(\omega_0't')]\Theta(t') \ . \tag{47}$$

That is, the electron moves almost as a classical particle, satisfying the (Newtonian) equation of motion

$$d^2x'(t')/dt'^2=-E'(t')=A_0'\omega_0'\cos(\omega_0't')\Theta(t') \ , \tag{48}$$

subject to the initial condition $x'(0)=0$ and

$$\left.\frac{dx'(t')}{dt'}\right|_{t'=0}=0 \quad (\text{for } \phi=0) \ .$$

The drift toward negative $\langle x'\rangle$ values observed in cases (1) and (2) occurs here also, but is much less apparent. This observable drift, in cases (1) and (2), is peculiar to our choice of phase ($\phi=0$) at $t'=0$. For example, if the phase were chosen instead to be π, then drift to-

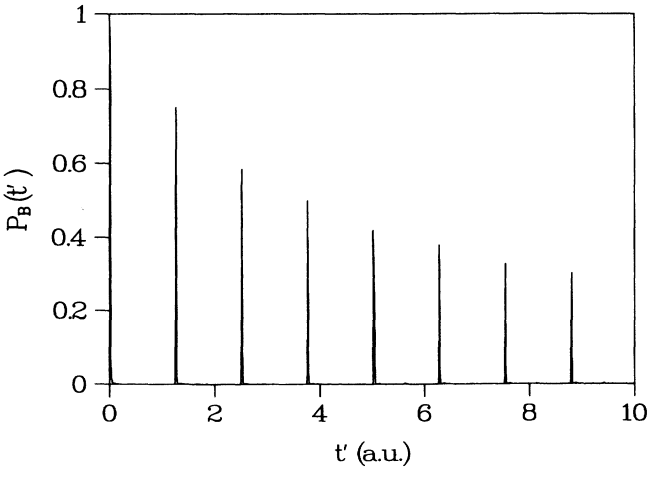

FIG. 10. $P_B(t')$ vs t', for $A_0'=30$, $\omega_0'=5$, and $\phi=0$.

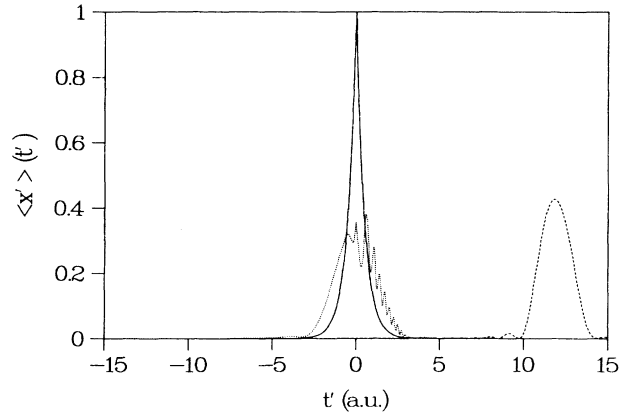

FIG. 11. $|\Psi(x',t')|^2$ vs x', for $t'=0$(——), π/ω_0'(— — —), and $2\pi/\omega_0'$(· · · ·); conditions as in Fig. 10.

ward positive x' values would occur. See further remarks following Eq. (56).

Presumably, as both A_0' and ω_0' grow larger, Eq. (47) will become more nearly an exact description of the motion of the center of the electronic wave packet. Observe that Eq. (47) is a very inaccurate description of electronic motion in cases (1a) and (1b). In those cases, although $\langle x'\rangle(t')$ does have the oscillatory behavior described by Eq. (47) (with the addition of a drift motion), the probability density does not show visible oscillations.

As is seen from the Fig. 10, $P_B(t')$ is periodic, the maxima decaying very slowly, approximately as $1/t'$, at very large t'. We propose, in this case, that $P_B(t')$ can be described approximately by projecting the bound-state wave function onto a spreading wave packet, the center of which executes the classical motion described by Eq. (47). In analogy to Eq. (19), we define this projection as

$$\Pi(t')\equiv\left|\int dx'\phi_B^*(x')\exp[ix'A(t)]\zeta(x',t')\right|^2, \quad (49)$$

where the oscillating semiclassical (Volkov) wave packet is given by

$$\zeta(x',t')=\int(dk/2\pi)\exp\{ik[x'-x_0(t')]-ik^2t'/2\}\xi_B(k) . \quad (50)$$

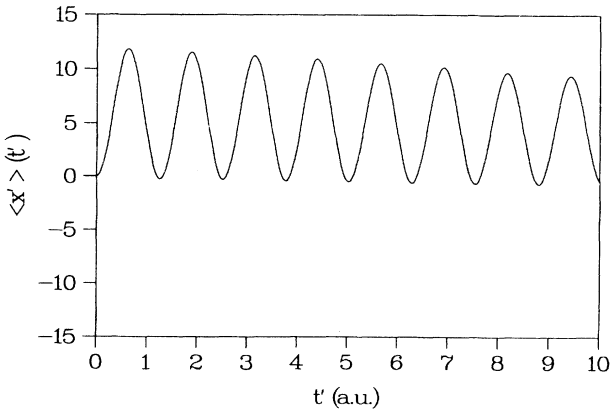

FIG. 12. $\langle x'\rangle(t')$ vs t'; conditions as in Fig. 10.

$x_0(t')$ is taken from Eq. (47), and $\xi_B(k)$ is the Fourier transform of $\phi_B(x)$. The initial spread in momenta is controlled by $\xi_B(k)$. Equation (49) can be rewritten as

$$\Pi(t')=\left|\int dk(1/2\pi)\exp\{-i[kx_0(t')+k^2t'/2]\}\times|\xi_B(k+A(t'))|^2\right|^2 . \quad (51)$$

In Fig. 13, we plot $\Pi(t')$ versus t' for $A_0'=30$ and $\omega_0'=5$. Results should be compared with Fig. 10. Obviously, one has that $\Pi(t')\approx P_B(t')$. We note that the expectation value of $x'(t')$ versus t', in the state $\zeta(x',t')$, is given exactly by Eq. (47); i.e.,

$$(A_0'/\omega_0')[1-\cos(\omega_0't')]=\int dx'\zeta^*(x',t')x'\zeta(x',t') . \quad (52)$$

The rms spread in this wave-packet state (ζ) is given by

$$[\langle x'^2\rangle(t')-\langle x'\rangle^2(t')]^{1/2}=[Z^4t^2+\tfrac{1}{2}]^{1/2}=[t'^2+\tfrac{1}{2}]^{1/2} , \quad (53)$$

where, in the first line, we have explicitly included the Z dependence. We repeat that, for this strongly coupled case, the motion of the electron described by Eq. (47) is very nearly classical. In particular, the amplitude of the oscillation (A_0'/ω_0') is given by the classical value, (if t' is not too large), while the maximum excursion experienced by the electron is $2A_0'/\omega_0'$.

The wave packet of Eq. (50) is the limit of the exact solution of the full Schrödinger equation [Eq. (3)], in the "modified Volkov-state basis," when continuum-continuum coupling between Volkov states is ignored; see Eq. (34) in the Volkov-State Basis section. Under the same conditions, the projection $\Pi(t')$ of Eq. (51) is equal to the limit of the exact $P_B(t')$ computed in the modified Volkov-state basis [Eq. (38)].

From this last observation, it is clear that the modified Volkov-state basis should yield a more economical calculation of $\Psi(x',t')$, than a calculation performed in a basis of eigenstates of the δ potential, for this case of large A_0' and large ω_0'. In fact, the calculation is at least ten times faster in the Volkov basis, for this [case (2)] choice of

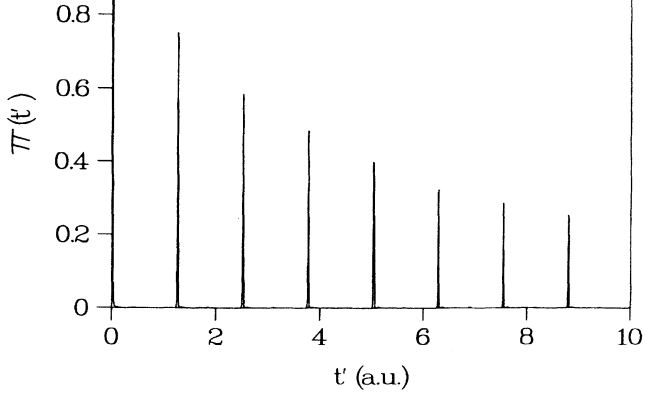

FIG. 13. $\Pi(t')$ vs t'; conditions as in Fig. 10.

laser parameters.

It would be misleading, however, to suppose that ionization always proceeds slowly in the semiclassical region; i.e., that $P_B(t')\sim 1/t'$. In fact, this is only so if we make the choice $\phi=0$. On the contrary, for $\phi\neq 0$, ionization can be very rapid, occurring in much less than a quarter of a laser cycle. We point out that the reason that ionization is so "slow," when $\phi=0$, is that the electron returns periodically to the origin with essentially zero velocity; i.e., just the value of (average) velocity it had at $t=0$. The initial bound state is thereby almost completely recomposed at the end of each half cycle, except for a between-times spreading of the wave packet.

To illustrate the ionization behavior when $\phi\neq 0$, we plot in Fig. 14 computed values of probability density versus x', for several t' values, when $\phi=\pi/2$ (and $A_0'=30$, $\omega_0'=5$). The corresponding values of $\langle x'\rangle(t')$ versus t' appear in Fig. 15. The expectation value of x', as well as the probability density, now mimic the more general classical trajectory described by

$$x'(t')=(A_0'/\omega_0')[\cos\phi-\cos(\omega_0't')-w_0't'\sin\phi]\Theta(t') , \tag{54}$$

where $\phi=\pi/2$, instead of Eq. (47), which pertained only for $\phi=0$. The trajectory described by Eq. (54) moves rapidly away from the origin, with a "drift" velocity given by

$$v_{\text{drift}}=-A_0'\sin\phi . \tag{55}$$

The probability of remaining in the bound state $P_B(t')$ is no longer periodic, but decays monotonically; see Fig. 16.

The classical drift velocity, described by Eq. (55), and clearly depicted in Fig. 15, is, however, not synonomous with the drifts appearing in Figs. 5, 9, and 12 (when $\phi=0$). Rather, we hypothesize that those drifts arise from a lag between the time of laser turn on, and the time at which the electron arrives in the continuum; i.e., a lag time comparable to τ_{PI}'. Indeed, assuming a classical equation of motion, modified by a "switching" function, of the form

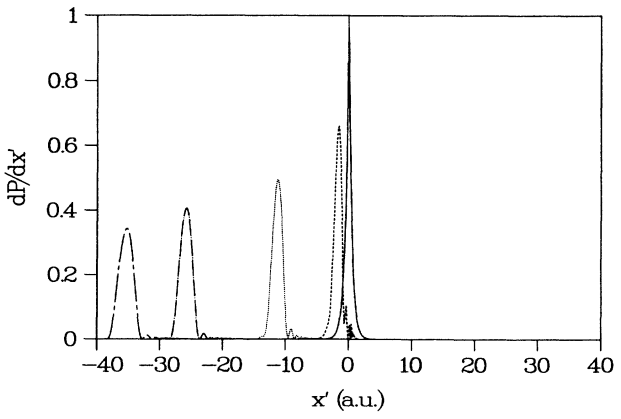

FIG. 14. $|\Psi(x',t')|^2$ vs x', for $t'=0$(——), 0.25(— — —), 0.50(· · · ·), 0.75(—·—·—·), and 0.99(—·—·-), and with $A_0'=30$, $\omega_0'=5$, and $\phi=\pi/2$.

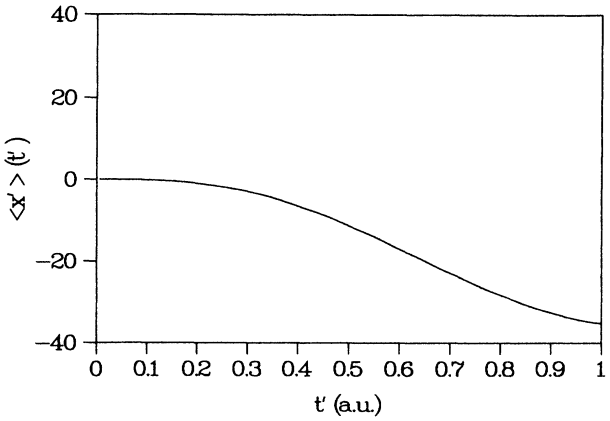

FIG. 15. $\langle x'\rangle(t')$ vs t'; conditions as in Fig. 14.

$$\frac{d^2x'(t')}{dt'^2}=-[1-\exp(-t'/\tau_{\text{PI}}')]A_0'\omega_0'\cos(\omega_0't')\Theta(t') \tag{56}$$

[instead of Eq. (48)], one computes a classical trajectory $x'(t')$ which is generally closely similar to the quantum expectation value, $\langle x'\rangle(t')$, even for small A_0'. In Fig. 17, we plot values of $\langle x'\rangle(t')$ versus t' obtained for $A_0'=0.25$ and $\omega_0'=0.6$ (identical to Fig. 5), and the classical trajectory implied by Eq. (56), for the same choice of laser parameters, when $\tau_{\text{PI}}'=32$.

Case (3): Field-ionization approximation ($I_0'<1$ and $I_0'/\omega_0'^2>1$)

Now ionization occurred "rapidly," $\tau_{\text{PI}}'<2\pi/\omega_0'$. As an example of this case, in Fig. 18 we plot $P_B(t')$ versus t' when $A_0'=8.0$ and $\omega_0'=0.04$.

This case could be understood by having recourse to the theory of static-field ionization.[18] The characteristic time for tunneling was determined to be, for a δ potential,

$$1/\tau_{\text{PI}}'=\exp(-\tfrac{2}{3}A_0'\omega_0') . \tag{57}$$

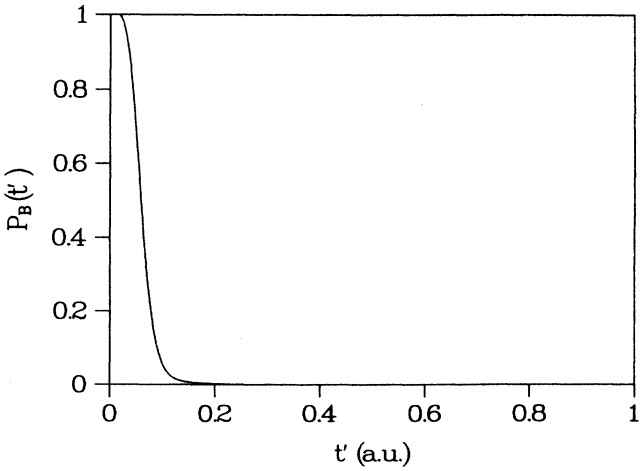

FIG. 16. $P_B(t')$ vs t'; conditions as in Fig. 14.

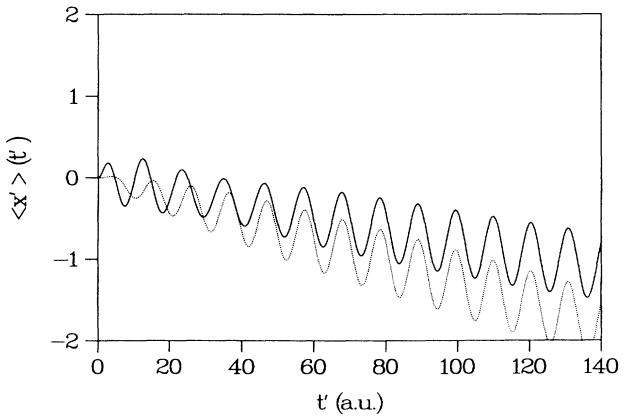

FIG. 17. $\langle x' \rangle(t')$ vs t', for $A_0'=0.25$, $\omega_0'=0.6$, and $\phi=0$ (——); $x'(t')$ vs t', for the same laser parameters, and with $\tau_{PI}'=32$ [from Eq. (56)] (· · · ·).

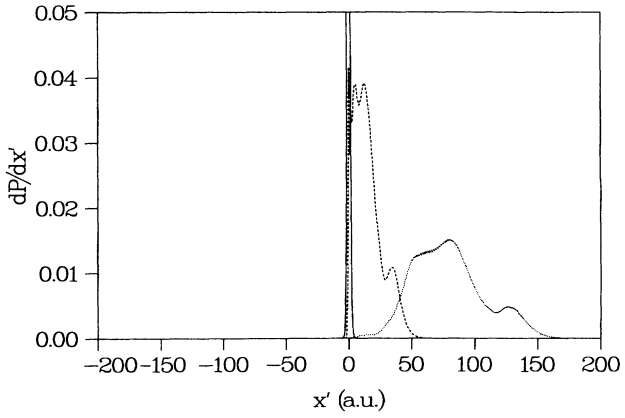

FIG. 19. $|\Psi(x',t')|^2$ vs x', for $t'=0$(——), 15(— — —), 30(· · · ·); conditions as in Fig. 18.

For the choice of parameters in this example, the tunneling time from Eq. (57) is $\tau_{PI}'=8.0$ to be compared with the "measured" value, from Fig. 18, of 9.7. This description becomes more accurate as ω_0' becomes smaller and A_0' becomes larger, so that ionization occurs in just a small fraction of a laser cycle (provided that $I_0'<1$). As ω_0' becomes larger and A_0' becomes smaller, a generalization of Eq. (57), for time-varying fields, may have some applicability.[18]

To further illustrate this case, in Fig. 19 we plot values of the probability density $|\Psi(x',t')|^2$ versus x', for three t' values. Figure 19 should be compared with its analog (Fig. 4), for $A_0'<1$. In Fig. 20, we plot the expectation value of x' versus t'. Contrasting with cases (1a), (1b), and (2), now oscillations in $\langle x' \rangle(t')$ are not well developed.

We emphasize that all of the results described in this section were obtained via calculations performed in both the $\mathbf{k}\cdot\mathbf{A}$ and $\mathbf{x}\cdot\mathbf{E}$ gauges. Consistency of results was achieved in every case, and constituted a check on the calculation. It is worth pointing out, however, that calculations were typically much more time consuming in the $\mathbf{x}\cdot\mathbf{E}$ gauge. The extent of continuum-continuum coupling required for convergence in the $\mathbf{xE}$ gauge was usually very large, whereas coupling in the $\mathbf{k}\cdot\mathbf{A}$ gauge could almost always be limited to a band of ~ 200 continua; i.e., in Eq. (14), the range of n' could usually be restricted to $n-100\le n'\le n+100$, where $n<1$ enumerates the continua [see Eq. (10)]. Calculations of $\langle x' \rangle(t')$ were particularly sensitive in this regard, the necessary range tending to grow with t'. The extent of continuum-continuum coupling, required to produce convergence, is a measure of the failure of the Reiss formula [Eq. (45)], which implies no such coupling.

Generally, when $A_0'<1$, $\mathbf{k}\cdot\mathbf{A}$ gauge calculations of $\Psi(x',t')$ could be performed very quickly in a basis of eigenstates of the δ potential. However, when $A_0'>1$, then extensive continuum-continuum coupling acted to slow the calculation in this basis. If $A_0'>1$ and $\omega_0'>1$, then the basis of modified Volkov states led to a very rapid calculation. The worst case was for $A_0'>1$ and $\omega_0'<1$, where both bases yielded very slow calculations.

The maximum number of states included in our calculations was 801. Positive and negative k' values were always included for each $|\mathbf{k}'|$. Generally, as A_0' increased, the range of required k' also increased. Equally significant, at large A_0', was the small time step required

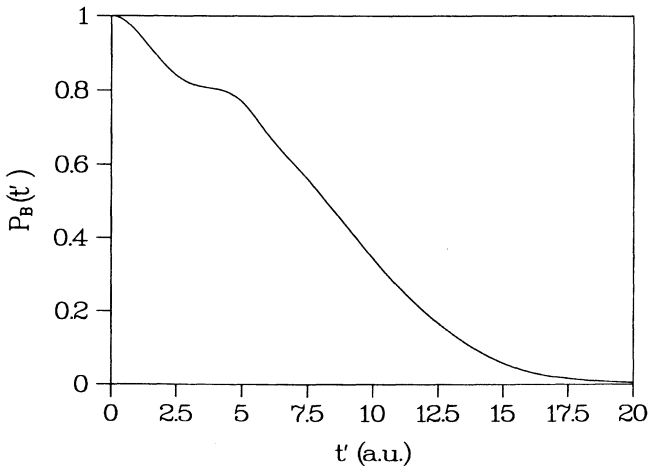

FIG. 18. $P_B(t')$ vs t', for $A_0'=8.0$, $\omega_0'=0.04$, and $\phi=0$.

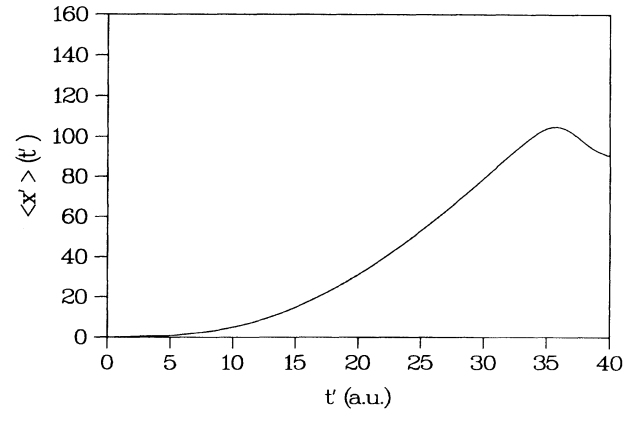

FIG. 20. $\langle x' \rangle(t')$ vs t'; conditions as in Fig. 18.

to generate the numerical solution.

We note that for each A'_0,ω'_0 combination, the total number of k' values included, and the minimum k' value [π/L', from Eq. (10)] employed, were selected such that (a) the range of k' values generated, with appreciable probability via coupling in Eq. (3) [or Eq. (14)], was spanned and (b) there was never any appreciable probability generated near the end of the box; i.e., for a given maximum t', L' was "large enough." In practice, these conditions were all satisfied only after having made several preliminary trial-and-error calculations.

DISCUSSION

The results described in the preceding section are typical of calculations we performed for a broad range of parameter (I'_0,ω'_0) choices. As mentioned, calculated values of the characteristic ionization time $\tau'_{\rm PI}$ could often be well approximated by having recourse to one of three simple methods, depending on the region of parameter space involved: The Reiss approximation [case (1)]; the semiclassical approximation [case (2)]; or the static-field-ionization formula [case (3)]. These conclusions are summarized schematically in Fig. 1, where the regions labeled 1–3 correspond to the same numbers from the Results section.

Region 4, of Fig. 1, labels a range of parameters (I'_0,ω'_0) where the semiclassical approach is clearly invalid, and both the Reiss and static-field-ionization formulas are questionable. Worse still, both Reiss and field ionization based predictions of $\tau'_{\rm PI}$ in this region typically exceed several tens of thousand a.u., so that complete numerical computations based on Eq. (3) are probably unfeasible here, at present. This assumption was verified by performing incomplete calculations, out to several thousand a.u. of time, for these cases.

Unfortunately, region 4 represents a range of (I'_0,ω'_0) values which is very interesting for laser-plasma modeling. For example, at a laser irradiance of $I_0=10^{19}$ W/cm^2 and photon energy $\omega_0=5$ eV, we compute, based on the Reiss formula [Eq. (45)], a value of $\tau_{\rm PI}=7.1\times10^{-12}$ sec, for the characteristic photoionization time of a $1s$ electron in Ar^{17+} (hydrogenlike argon). For this choice of parameters (I_0, ω_0, and $Z=18$), one has that $A'_0=5.08$ a.u. and $\omega'_0=0.000\,567$ a.u.; i.e., this point lies in region 4. The predicted photoionization time, in scaled units, is $\tau'_{\rm PI}=9.1\times10^7$ a.u. But, since the maximum quiver energies generated in this case are of the order of 10 a.u., the step size required in a numerical solution of Eq. 3 must be very much smaller than 0.1. The severity of the numerical problem, in this region, is obvious.

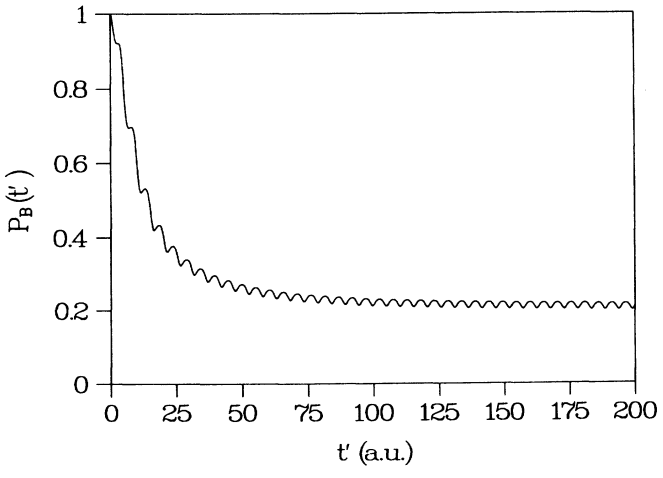

FIG. 21. $P_B(t')$ vs t', for $A'_0=0.5$ and $\omega'_0=0.6$.

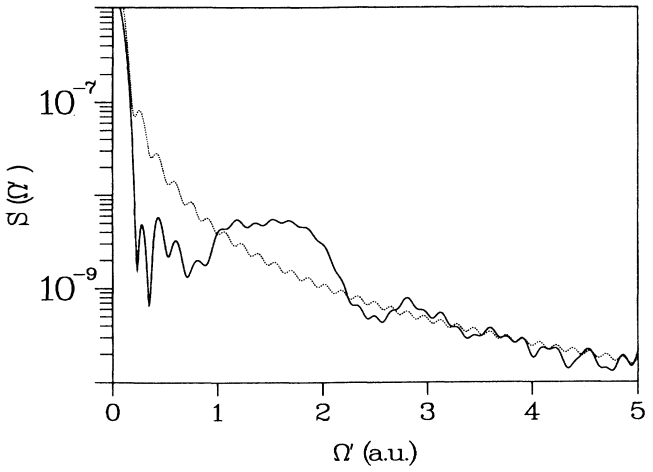

FIG. 22. $S(\Omega')$ vs Ω'; conditions as in Fig. 18.

We should point out that there is currently no empirical evidence of a ponderomotive shift [last term on the right-hand side of Eq. (46)] for ionization occurring under these "exotic" conditions (large A'_0, but small ω'_0). But the prediction of the Reiss formula [Eq. (45)] can be very sensitive to the assumption that such a shift exists. For instance, if this shift is omitted from Eq. (46), then Eq. (45) predicts a value of the characteristic photoionization time of $\tau'_{\rm PI}=0.21\times10^{-12}$ sec, for the conditions outlined in the preceding paragraph.

In the vicinity of an energy threshold, the detailed numerical results showed a sometimes drastic slowing down of ionization, not usually well represented by any of the approximations. This slowing down of ionization near a threshold, is evidently typical of short-range potentials. The Coulomb potential, of course, does not show a slowing down. For example, in Fig. 21 we plot values of $P_B(t')$ versus t' for the case $A'_0=0.5$, $\omega'_0=0.6$.

From the present vantage point, it seems worthwhile to reconsider briefly the topic of indirect photoionization. In a multielectron atom or ion, collision between a deeply bound electron and an outer-shell or weakly bound electron which is quivering in the laser field may conceivably result in an enhanced ionization rate.[11,13] Based on our results, we propose that such an effect will occur most readily when both $A'_0\gg1$ and $\omega'_0\gg1$. This is for two reasons: (a) The (maximum) ponderomotive energy $A'^2_0/2$, is the maximum energy transferable in a (single) collision. Consequently, A'_0 must be large, albeit not so large that the collision cross section becomes small. If instead $A'_0<1$, then quiver motion is inherently low energy even though, if $\omega'_0\ll1$, it could have large amplitude.

[From Eq. (47), the amplitude is A'_0/ω'_0.] (2) If both $A'_0 \gg 1$ and $\omega'_0 \gg 1$, then quiver motion, in the form of dipole charge-density oscillations, will be well developed throughout the ionization process [see case (2) of the Results section]. On the other hand, if $A'_0 \gg 1$ but $\omega'_0 \ll 1$, then dipole charge-density oscillations are ill formed during ionization [see case (3) of Results section]. If $A'_0 < 1$, then although $\langle x' \rangle(t')$ oscillates as a function of t', the probability density is almost symmetrical about $x'=0$; i.e., dipole charge-density oscillations are poorly formed during ionization, and the electron has a vanishingly small probability of remaining in the vicinity of the origin.

It may be useful to remark[19,20] that, during and after ionization, a "classical" electron entrained in the laser field will radiate electromagnetic energy at the rate[21]

$$\mathcal{P}(t')=(2\alpha^3/3)|d^2x'(t')/dt'^2|^2 , \tag{58}$$

in a.u. where α is the fine-structure constant and $\mathcal{P}$ is the power. If the electron were "free" and completely nonrelativistic, then all emitted radiation would be (Thomson) scattered at the fundamental laser frequency.[21] In our example, however, radiation at other than the fundamental frequency is induced by both the transient ionization behavior and the abrupt turn on of the laser.

In this paper, we have described the quantum-mechanical motion of an initially bound electron being ionized by a laser field. Ignoring radiation damping, we take the spectral density of energy radiated classically by such an electron to be,[21] in a.u., and with scaled variables,

$$\begin{aligned} S(\Omega') &\equiv (\alpha^3/3\pi)\left| \int dt' \exp(i\Omega' t') d^2\langle x' \rangle(t')/dt'^2 \right|^2 \\ &= (\alpha^3/3\pi)\left| \int dt' \exp(i\Omega' t')\{ dA'(t')/dt' + \langle [[H',x'],H'] \rangle(t') \} \right|^2 \\ &= (\alpha^3/3\pi)\left| \int dt' \exp(i\Omega' t')\{ A'_0 \omega'_0 \cos(\omega'_0 t') - d|\Psi(x',t')|^2/dx'|_{x'=0} \} \right|^2 , \end{aligned} \tag{59}$$

having twice used the fact that $dO/dt = i[H,O] + \partial O/\partial t$, where O is any operator, and $[H,O]$ is the commutator of O with the full Hamiltonian H appearing in Eq. (3) ($\mathbf{k}\cdot\mathbf{A}$ gauge). The units of $S(\Omega')$ are energy per unit energy per ionization event. Radiation damping can be ignored whenever $\alpha^3\omega'_0 << 1$.

From Eq. (59), we computed the spectral density of radiation emitted by an initially bound electron moving in a laser field with parameters $A'_0=8.0$ and $\omega'_0=0.04$; the choice of parameters corresponds to case (3) of the Results section. The generated spectrum appears in Fig. 22 (solid curve). For comparison, a spectrum corresponding to the purely classical trajectory of Eq. (47), with $0 \le t' \le 40$, is also plotted (dotted line). In both curves, the most rapid oscillations are due to the sharp cutoff in the time record at $t'_{\max}=40$ (and the sharp turn on at $t'=0$; i.e., those oscillations with period $2\pi/t'_{\max} \approx 0.16$.

More importantly, in the classical case (dotted curve), the slow falloff of $S(\Omega')$ with increasing Ω' can be shown to be due solely to the abrupt turn on of the laser. From this fact, and the similarity of the two curves, we conclude that, in the quantal calculation, the effect of transient ionization behavior on $S(\Omega')$ must be small, at large Ω', for this choice of laser parameters. Of course, in any real experiment, in which laser turnon would not be abrupt, $S(\Omega')$ would decrease more rapidly, with increasing Ω', than implied by Fig. 22.

SUMMARY

In this paper, we have described the effect of a classical single-frequency laser field on the quantum-mechanical motion of an electron, moving in the field of a δ potential and bound initially by that potential. A characteristic time for photoionization $\tau'_{\rm PI}$ was computed for the electron, over a wide range of scaled laser parameters, I'_0 and ω'_0, where $I'_0=I_0/Z^6$ and $\omega'_0=\omega_0/Z^2$, and $-Z^2/2$ is the bound-state energy. Values of $\tau'_{\rm PI}$ obtained from these detailed calculations were compared with predictions made by three different approximations. ATI spectra of the ionized electron were computed, as well as the spectral density of emitted radiation. The conditions under which well-defined electron quiver motion appears were clarified.

ACKNOWLEDGMENTS

The author wishes to thank G. Steven Vanni, of U.S. Naval Academy, for his very valuable help in doing the bulk of the Cray XMP supercomputer–based coding. Thanks also to Jack Comly, of LANL, for many helpful discussions of physics questions, and to Gordon Olson, also of LANL, for providing an efficient differential equation solver.

[1]H. Reiss, J. Opt. Soc. Am. B **4**, 726 (1987).
[2]S. Geltman, J. Phys. B **10**, 831 (1977).
[3]E. Austin, J. Phys. B **12**, 4045 (1979).
[4]S. Susskind and R. Jensen, Phys. Rev. A **38**, 711 (1988).
[5]B. Sundaram and L. Armstrong, Phys. Rev. A **38**, 152 (1988).
[6]L. Collins and A. Merts, Phys. Rev. A **37**, 2415 (1988).
[7]K. Kulander, Phys. Rev. A **38**, 778 (1988).
[8]J. Javanainen, J. Eberly, and Q. Su, Phys. Rev. A **38**, 3430

(1988).
[9]K. LaGattuta, G. Olson, and J. Comly, Bull. Am. Phys. Soc. **33**, 1042 (1988).
[10]J. Cobble, G. Kyrala, A. Hauer, A. Taylor, C. Gomez, N. Delamater, and G. Schappert, Phys. Rev. A **39**, 454 (1989).
[11]P. Lee, D. Casperson, and G. Schappert (unpublished).
[12]P. Lambropoulous, Phys. Rev. Lett. **55**, 2141 (1985).
[13]K. Boyer and C. Rhodes, Phys. Rev. Lett. **54**, 1490 (1985).
[14]J. Javanainen and J. Eberly, Phys. Rev. A **39**, 458 (1989).
[15]M. Mittleman, *Theory of Laser-Atom Interactions* (Plenum, New York, 1982).
[16]P. Agostini, F. Fabre, G. Maimfray, G. Petite, and N. Rahman, Phys. Rev. Lett. **42**, 1127 (1979).
[17]D. Volkov, Z. Phys. **94**, 250 (1935).
[18]A. Perelomov, V. Popov, and M. Terentev, Zh. Eksp. Teor. Fiz. **50**, 1393 (1966) [Sov. Phys.—JETP **23**, 924 (1966)].
[19]J. Eberly (private communication).
[20]M. Ferray, A. L'Huillier, X. Li, L. Lompre, G. Mainfray, and C. Manus, J. Phys. B **21**, L31 (1988).
[21]J. Jackson, *Classical Electrodynamics* (Wiley, New York, 1967).
[22]L. Landau and E. Lifshitz, *Quantum Mechanics* (Addison-Wesley, Reading, MA, 1958).